

## THE CORRELATION BETWEEN METALLICITY AND DEBRIS DISK MASS

ANDRÁS GÁSPÁR<sup>1</sup>, GEORGE H. RIEKE<sup>1</sup>, AND NICHOLAS BALLERING<sup>1</sup>

1) Steward Observatory, University of Arizona, Tucson, AZ, 85721  
agasp@as.arizona.edu, griek@as.arizona.edu, ballerin@email.arizona.edu

April 27, 2016

### ABSTRACT

We find that the initial dust masses in planetary debris disks are correlated with the metallicities of their central stars. We compiled a large sample of systems, including *Spitzer*, the Herschel DUNES and DEBRIS surveys, and *WISE* debris disk candidates. We also merged 33 metallicity catalogs to provide homogeneous  $[\text{Fe}/\text{H}]$  and  $\sigma_{[\text{Fe}/\text{H}]}$  values. We analyzed this merged sample, including 222 detected disks (74 warm and 148 cold) around a total of 187 systems (some with multiple components) and 440 disks with only upper limits (125 warm and 315 cold), around a total of 360 systems. The disk dust masses at a common early evolutionary point in time were determined using our numerical disk evolutionary code, evolving a unique model for each of the 662 disks backward to an age of 1 Myr. We find that disk-bearing stars seldom have metallicities less than  $[\text{Fe}/\text{H}] = -0.2$  and that the distribution of warm component masses lacks examples with large mass around stars of low metallicity ( $[\text{Fe}/\text{H}] < -0.085$ ). Previous efforts to find a correlation have been largely unsuccessful; the primary improvements supporting our result are: 1.) basing the study on dust masses, not just infrared excess detections; 2.) including upper limits on dust mass in a quantitative way; 3.) accounting for the evolution of debris disk excesses as systems age; 4.) accounting fully for the range of uncertainties in metallicity measurements; and 5.) having a statistically large enough sample.

**Keywords:** methods: numerical – circumstellar matter – planetary systems – infrared: stars

### 1. INTRODUCTION

The past three decades have seen the discovery of hundreds of planetary debris disks (e.g., Wyatt 2008) and a multitude of planets, either via radial-velocity surveys (e.g., HARPS - Mayor et al. 2009), transit surveys (e.g., Kepler - Borucki et al. 2010), microlensing (e.g., Bennett et al. 2006), or direct imaging (e.g., Marois et al. 2008). Together these discoveries have promoted exoplanetary system astronomy to a very prominent field of study. However, each of these tools probes only a small part of exoplanetary system behavior, and to understand more we need to combine these individual insights (e.g., Wright & Gaudi 2013).

Circumstellar planetary debris disks (e.g., Smith & Terrile 1984; Backman & Paresce 1993) have the potential to probe: 1.) the evolution of the populations of small bodies, e.g. exoasteroids and exo-Kuiper-Belt-objects; 2.) recent major stochastic events such as exoasteroid collisions; 3.) placement of critical zones, such as ice lines; and 4.) indirect indications of the existence and placement of planets.

For example, we see debris disks fade at rates consistent with monotonic evolution from a formative stage, consistent with expectations for collisional cascades within exoasteroidal belts, similar to the behavior of our asteroids (Wyatt et al. 2007; Gáspár et al. 2013). In some cases, particularly in young systems, there is direct evidence for huge collisions, either through spectral features indicative of fine silica dust (e.g., Johnson et al. 2012) or other very finely divided crystalline material, or through variability (e.g., Meng et al. 2014). Imaged disks often show two distinct planetesimal zones analogous to the asteroid and Kuiper Belts (e.g., Acke et al. 2012; Su et al. 2013) and many unresolved systems have temperature structures suggestive of a similar dual disk structure (e.g., Morales et al. 2011; Ballering et al. 2013; Chen et al. 2014). These structures may reflect ice line positions in the ancestral protoplanetary disks, with subsequent

modification of the disk structure by planets. In fact, the putative planets have been imaged in some debris disk systems (Fomalhaut, HR 8799,  $\beta$  Pic, HD95086, FW Tau, ROXs 12, ROXs 42B, HD 106906 Kalas et al. 2008; Marois et al. 2008; Lagrange et al. 2010; Moór et al. 2013; Kraus et al. 2014; Currie et al. 2014; Bailey et al. 2014). The architectures of the disks in these systems are generally in agreement with the predictions from current disk – planet interaction models (e.g. Chiang et al. 2009; Rodigas et al. 2014).

The influence of metallicity as measured by  $[\text{Fe}/\text{H}]$  can in principle provide additional insights to planetary system formation and evolution, especially as an indicator of other heavy elements, such as the building blocks of organic molecules and planets (C, N, O, Si). As an example, the discovery that the number of massive, hot planets increases rapidly with increasing metallicity (e.g., Fischer & Valenti 2005; Johnson et al. 2010), in qualitative agreement with expectations, has inspired many hypotheses for the exact mechanism responsible (e.g., Johansen et al. 2009; Garaud 2011; Johnson & Li 2012; Cossou et al. 2014; Nayakshin 2015). How varying opacity affects - if at all - planet formation is still debated in planet formation theory. While higher metal content is an indication of a generic higher density of available building material in the systems, it also may play a crucial role in the physics driving planet formation itself. While Boss (2002) found only negligible variations in his gravitational instability models, Cai et al. (2006), Meru & Bate (2010), and Gammie (2001) find that lower metallicity systems cool faster and fragment more, aiding core accretion processes. This, however, also means that proto-planets in metal rich systems may have more time to accrete matter and form giant planets.

On first principles, higher metallicity should also favor the development of massive debris disks, since the necessary raw materials are then more abundant. Indeed, if the numbers of debris parent bodies are proportional to the metallicity, the prominence of debris disks might increase faster than pro-

**Table 1**

Properties and sources of the targets analyzed in the study. Stellar parameters were determined via model spectra fitting. Disk catalogs are coded as follows: **DUNES**, **DEBRIS**, **K. Su et al. (2006)**, **N. Ballering et al. (2013)**, **J. Sierchio et al. (2013)**, and **WISE**. Only the first 10 lines are displayed, the full table is available online at ApJ or at CDS.

Name HIP	HD	Catalog	d (pc)	$M_*$ ( $M_\odot$ )	$L_*$ ( $L_\odot$ )	$R_*$ ( $R_\odot$ )	Age (Gyr)
000490	000105	JS,NB	39.4	1.13	1.29	1.06	0.170
000544	000166	DU,NB,W	13.7	0.98	0.60	0.94	0.240
000560	000203	NB	39.4	1.45	4.20	1.51	0.012
000682	000377	JS,NB	39.1	1.11	1.17	1.09	0.220
000910	000693	DU	18.7	1.39	3.07	1.50	3.000
000950	000739	DE	21.3	1.39	3.05	1.38	2.150
001031	000870	JS,NB	20.2	0.93	0.48	0.84	2.300
001134	000984	JS	47.1	1.27	2.14	1.25	0.250
001292	001237	DE	17.5	0.99	0.64	0.88	0.300
001368	-	DE,NB	15.0	0.65	0.11	0.68	0.900

tionately since the collision rates should go roughly as the square of the space density of parent bodies. These trends might be countered if the sinks for planetesimals - assimilation into planets, or ejection from the system - have a countervailing dependence on metallicity. However, the numbers of the planets in the most common mass range - super-Earths to Neptunes (Malhotra 2015) - have at most a weak dependence on metallicity (e.g., Sousa et al. 2011b; Buchhave et al. 2014; Wang & Fischer 2015). Thus, as direct sinks for planetesimal raw material they should have a neutral effect, or perhaps even reduce the available material at low metallicity. The fraction of stars with Jupiter-mass planets is low,  $\lesssim 1\%$  (e.g., Wang et al. 2015; Malhotra 2015), so it would be surprising if their prowess at ejecting planetesimals had a noticeable effect on the overall incidence of debris disks.

Despite these arguments, virtually all searches for a relation between stellar metallicity and the presence of debris disks (e.g., Bryden et al. 2006; Beichman et al. 2006; Greaves et al. 2006; Trilling et al. 2008; Marshall et al. 2014; Thureau et al. 2014) find none. Maldonado et al. (2012) report a hint of a deficit of disks at low metallicity, but this behavior was not confirmed in a later paper (Maldonado et al. 2015), possibly because of the smaller sample in the latter work. Within the errors, these works are consistent with the incidence of debris disks being independent of the stellar metallicity<sup>1</sup>.

With the exception of those by Maldonado et al. (2012, 2015), these previous searches for a metallicity/debris disk relation have each been based on no more than  $\sim 40$  detected debris disk systems. Any systematic effects must be recognized out of a huge range of disk-creating activity, disk evolutionary behavior, and significant measurement errors, placing a premium on averaging down the scatter with large numbers and on minimizing systematic effects. The era of major space-based surveys for debris disks is now past (with the demise of IRAS, ISO, cryo-Spitzer, Akari, cryo-WISE, and Herschel). It is therefore timely to combine the results from these missions to gain significantly in the statistical significance of debris disk studies. The study reported here is based on a combined catalog of 662 systems, including 222 detected examples and 440 meaningful upper limits.

We also introduce new approaches to reduce systematic effects. To be specific, the previous studies simply compared the stellar metallicity distribution of sources with or without

detected excesses of any size, whereas it is the disk masses that should correlate with metallicity. Furthermore, the previous work does not take debris disk evolution into account which, if ignored, will dilute any other effects on disk incidence because after a certain age stars of all metallicities will have few debris disks. Thus, a more sensitive search for a correlation between metallicity and the presence of debris disks should convert the debris disk emission levels to mass, correct to a common time, preferably one at a young age where the result should be representative of the dust mass in the protoplanetary disk (Wyatt et al. 2007; Gáspár et al. 2013), and work with the full distribution of detected masses and upper limits. It would also be desirable to treat separately the warm and cold debris disk components (Morales et al. 2011; Kennedy & Wyatt 2014) that evolve independently and at quite different rates (Gáspár et al. 2013). In this paper, we introduce all of these improvements. We also review the previous assumptions (e.g., on metallicity determination vs. spectral type) to identify any that might have undermined detection of an effect. Because of the new modeling approach and the large sample, we do find a dependence of disk mass on metallicity for both warm and cold disk components, at modest statistical significance.

We present this work as follows. In section 2, we detail the observational sample we use for our study, while in section 3 we describe the methods used to estimate the metallicities of the sources in the sample. The modeling methods are elaborated in section 4, while in section 5 we discuss the results. Section 6 summarizes our findings.

## 2. THE DISK SAMPLE

To build the largest possible sample of debris disks, we merged data from multiple sources. We separate the final sample into two groups: warm and cold debris disks. Systems with *Spitzer* 24  $\mu\text{m}$  excesses or upper limits or with WISE W4 excesses are included in the warm disk sample, while systems with *Spitzer* 70 and/or *Herschel* 70/100  $\mu\text{m}$  data (either excesses or upper limits) are included in the cold disk sample.

In the following subsections we detail each dataset used to compile our final warm and cold disk samples. For the study of warm disk components, based on our results in Gáspár et al. (2013), we selected only systems up to 0.5 Gyr in age, as detectable systems older than this limit are very likely to have undergone a recent collisional event. We also analyze the cold sample including only sources up to 5 Gyr in age, due to similar evolutionary effects recognized in Sierchio et al. (2014). For sources where disks were not detected at either 24  $\mu\text{m}$  (MIPS/*Spitzer* data) or at 70/100  $\mu\text{m}$  (MIPS/*Spitzer* or PACS/*Herschel* data), we used the upper limits given by the observations. From the *ROSAT* and *WISE* selected sample we only used the detections<sup>2</sup>. Our final disk catalog is shown in Table 1, with stellar mass, luminosity, and radius estimates from spectral model fitting.

### 2.1. The *Spitzer* IRS Selected Debris Disks

Ballering et al. (2013) analyzed *Spitzer* IRS spectra and MIPS 24 and 70  $\mu\text{m}$  data of 546 main sequence stars, characterizing 170 cold and 117 warm disk components of 214 sources with excess. A similar analysis of the IRS sample was performed by Chen et al. (2014). Ballering et al.

<sup>1</sup> Marshall et al. (2014) even find preliminary evidence for an inverse correlation.

<sup>2</sup> The *WISE* sample would have yielded a huge number of sources to run upper limit models for, and would not have contributed significantly to our results because these limits are generally less stringent than those from *Spitzer*.

(2013) specifically categorized debris disk systems as having either a warm and/or cold component and specific fluxes for each component are given, therefore, sources from the Ballering et al. (2013) IRS sample are included using their definitions and fluxes. We refer the reader to Ballering et al. (2013) for the details on how the temperatures of the components and the ages of the systems were determined. We required the sources in our study to have defined ages and metallicities, which narrowed the Ballering et al. (2013) sample to 140 systems with excesses (48 warm and 112 cold components and 36 and 28 upper limits, respectively)<sup>3</sup>.

## 2.2. The Gáspár et al. (2013) Sample

In Gáspár et al. (2013), we analyzed the *Herschel* DEBRIS and DUNES surveys (Eiroa et al. 2013; Thureau et al. 2014; Moro-Martín et al. 2015), and supplemented the *Herschel* results with *Spitzer* MIPS 24 and 70  $\mu\text{m}$  data. The Gáspár et al. (2013) results also included MIPS 24 and 70  $\mu\text{m}$  photometry from Sierchio et al. (2014) and Su et al. (2005), which we include in our current sample as well; however, we do not include stellar open cluster data. We took ages from Gáspár et al. (2013) and Sierchio et al. (2014) but updated the *Herschel* flux measurements with those from Eiroa et al. (2013), Thureau et al. (2014), and Moro-Martín et al. (2015). Of the 387 systems included from the Gáspár et al. (2013) sample, 60 are also part of the Ballering et al. (2013) IRS sample; the radial distances of the disks around them and the warm and/or cold disk flux contributions to their excesses were included from the IRS analysis. Excluding the IRS sources, 327 were included from the Gáspár et al. (2013) sample that had age and metallicity values, of which 105 were up to 500 Myr old.

## 2.3. The ROSAT and WISE selected Sample

In section 3, we compile a list of metallicity catalogs that had data for at least one of the sources either from the IRS or Gáspár et al. (2013) datasets. The combined non-redundant source count of these metallicity catalogs was 20811. Of the 20811 sources in the compiled catalog of sources with a metallicity value, essentially all have been measured with WISE and 1753 had ROSAT measurements. We used the latter to determine stellar ages, as in Sierchio et al. (2014)

$$\log_{10}(\tau/\text{yr}) = 1.2 - 2.307 \log_{10}(R_x) - 0.1512 [\log_{10}(R_x)]^2, \quad (1)$$

where  $R_x$  is the ratio of the X-ray to total luminosity:

$$R_x = 10^{20} \frac{L_x}{L}. \quad (2)$$

This age estimate is accurate to within 0.1-0.2 dex (Mamajek & Hillenbrand 2008; Sierchio et al. 2014). X-ray fluxes were calculated from HR1 *ROSAT* data following Schmitt et al. (1995), while total luminosities were estimated from SED fits. A total of 1736 sources had ROSAT, WISE, and metallicity data. The distribution of the W3-W4 colors peaked at 0.054 mag, with a rms scatter of 0.042 mag. Any source in the sample that had  $W3 - W4 \geq 0.181$  (i.e., a nominal  $3\text{-}\sigma$  detection) was further analyzed. If its excess at W4 was above the predicted levels by  $4\sigma_{W4}$  (using its individual measured error) and if its SED fit passed a by-eye examination for consistency, we added the source to our study. Only

59 sources passed all of these criteria. Of these, only 40 were younger than 0.5 Gyr; of the remaining 19, 5 were identified in other catalogs and further selected for the cold disk studies (as either detections or upper limits).

Similar WISE catalog searches were performed by Patel et al. (2014), Wu et al. (2013), and Cruz-Saenz de Miera et al. (2014). Patel et al. (2014) searched for WISE excess (W3 and W4) sources within 75 pc, placing special emphasis on finding sources with saturated photometry. Wu et al. (2013) searched for excesses at W4 for Hipparcos sources within 200 pc, while Cruz-Saenz de Miera et al. (2014) placed a photometry limit of  $V = 15^{\text{mag}}$  on their WISE catalog search. Of the 59 sources we identified, 57 are within 200 pc (compared to the 103 new detections by Wu et al. (2013)), 41 are within 75 pc (compared to the 106 new detections by Patel et al. (2014)), and all are brighter than  $V=10.12$  mag (well above the Cruz-Saenz de Miera et al. (2014) cutoff). Of the 59 sources we initially identified 27 were also found by either the Wu et al. (2013) or the Patel et al. (2014) analysis (or by both), however, 32 are possibly new sources. Patel et al. (2014) go through a rigorous set of 15 criteria that their data have to meet to be considered an excess source. To ensure that our data meet their criteria as well, we removed the new sources from our analysis as well as the sources that were older than 0.5 Gyr and only identified in the *ROSAT*/*WISE* sample. This finally leaves only 29 sources in this sample, of which 20 are younger than 0.5 Gyr. Of these 20, 11 are exclusively identified in the WISE study. This sequence of steps demonstrates that our sample is not missing a large number of strong WISE detections.

## 3. METALLICITIES

To determine the metallicities of the sources, we first compiled a list of all catalogs that had data for at least one of our stars. Some catalogs themselves were compilations (e.g. the PASTEL catalog - Soubiran et al. 2010 or Taylor 2005), while a few contained sources republished multiple times (e.g. the HARPS papers, Sousa et al. 2008, 2011a,b) or superseded/revaluated data (e.g. the Geneva-Copenhagen Survey, Nordström et al. 2004; Holmberg et al. 2009; Casagrande et al. 2011). We made sure to include data from each observation only once - the latest - in these cases, or in the case of the compilation catalogs to use them as aids in finding additional catalogs that were missing from Vizier. Our final database is assembled using 33 catalogs.

The metallicity values determined in each spectroscopic survey depend on instrument calibration, the lines used, whether  $[\text{Fe}/\text{H}]$  or total metallicity  $[\text{M}/\text{H}]$  is determined, and the synthetic model atmospheres that the observations are compared to. Because of these, catalogs may experience a metallicity-dependent scaling offset. To correct for this, before combining the catalogs, we converted the values from each catalog into a “common system”, which we chose to be that of Valenti & Fischer (2005). The conversion was performed by simple linear regression between the data sets, as  $[\text{Fe}/\text{H}]_{\text{merged}} = a + b[\text{Fe}/\text{H}]_{\text{original}}$ . We merged the catalogs together sequentially, in the order of the number of common sources between them and the sequentially merged catalog, recalculating the errors in metallicity as the rss of the errors in each catalog and the average of the metallicities weighted by their errors. The conversion factors were calculated preceding each sequential merging to ensure a larger number of points in the linear regression.

<sup>3</sup> We also removed the HIP 106741 system from the Ballering et al. (2013) sample, due to it likely being background contaminated (Panić et al. 2013).

**Table 2**

The metallicity catalogs combined in our work listed in the order of merging. Linear conversion factors ( $[\text{Fe}/\text{H}]_{\text{merged}} = a + b([\text{Fe}/\text{H}]_{\text{original}})$ ) are also given.

Sequence	Catalog	$a$	$b$	Notes
1	Valenti & Fischer (2005)	0.000	1.000	Base system in this study; spectroscopic; has common errors of $\sigma_{[\text{Fe}/\text{H}]} = 0.03$
2	Wu et al. (2011)	0.027	1.033	1273 stars; spectroscopic
3	Takeda et al. (2005)	0.003	0.966	160 mid-F to early K stars, spectroscopic
4	HARPS (Sousa et al. 2008, 2011a,b)	0.000	1.000	Spectroscopic, common sources were adopted from the latest papers
5	Robinson et al. (2007)	-0.009	0.885	N2K low-res spectroscopic survey, 1907 stars, $\sigma_{[\text{Fe}/\text{H}]} = 0.07$ used for all sources
6	Geneva-Copenhagen Survey (Casagrande et al. 2011)	-0.001	0.967	Latest, updated values of the spectroscopic survey data
7	Suchkov et al. (2003)	0.040	0.760	$[\text{Fe}/\text{H}]$ calculated from Strömgren photometry, based on Schuster & Nissen (1989)
8	NStars survey (Gray et al. 2003, 2006)	0.045	1.030	NStars spectroscopic survey of stars earlier than M0 and closer than 40 pc
9	Maldonado et al. (2012)	0.015	0.910	Only new spectroscopic data from Table 5 merged
10	Jenkins et al. (2008)	0.005	0.964	High-res spectroscopic survey of 353 solar-type stars
11	Koleva & Vazdekis (2012)	-0.002	0.939	Fitting of the New Generation Stellar Library (STIS/HST)
12	Bond et al. (2006)	0.091	1.330	High-res spectroscopic study of 136 G-type stars
13	Erspamer & North (2003)	0.027	0.970	High-res spectroscopic study of 140 A-F type stars
14	Saffe et al. (2008)	0.070	0.850	Spectroscopic study of 113 BAFGK-type Southern stars
15	Takeda et al. (2009)	0.040	0.950	Spectroscopic study of 120 A-type stars
16	Gerbaldi et al. (2007)	-0.020	0.660	$[\text{Fe}/\text{H}]$ calculated from Strömgren photometry
17	Gebran et al. (2010)	0.000	1.000	Spectroscopic study of 44 A and F-type Hyades stars
18	Katz et al. (2011)	-0.015	0.915	Spectroscopic study of 400 stars
19	Paulson & Yelda (2006)	0.015	1.760	Spectroscopic study of $\beta$ Pic MG stars, errors of $\sigma_{[\text{M}/\text{H}]} = 0.08$ used
20	Paunzen et al. (2002)	-0.190	0.893	Spectroscopic study of $\lambda$ Boötis stars
21	Kunzli & North (1998)	0.080	1.520	$[\text{M}/\text{H}]$ values adopted, with generic $\sigma_{[\text{M}/\text{H}]} = 0.2$
22	Philip & Egret (1980)	-0.056	0.691	$[\text{Fe}/\text{H}]$ from Strömgren photometry, with generic errors of $\sigma_{[\text{M}/\text{H}]} = 0.15^\dagger$
23	Gebran & Monier (2008)	0.070	1.000	High-res spectroscopic study of the Pleiades.
24	Jenkins et al. (2009)	0.000	1.000	Not enough data to determine conversion
25	Andrievsky (1998)	0.000	1.000	Not enough data to determine conversion
26	Guillout et al. (2009)	0.000	1.000	Not enough data to determine conversion
27	Lemke (1989)	0.000	1.000	Not enough data to determine conversion
28	Gebran et al. (2008)	0.000	1.000	Not enough data to determine conversion
29	Fuhrmann (2008)	0.016	0.938	Volume limited spectroscopic study of F-K stars
30	Favata et al. (1997)	-0.005	0.957	Spectroscopic study of 91 G and K stars
31	Luck & Heiter (2005)	0.004	0.892	Spectroscopic study of 114 stars within 15 pc
32	Luck & Heiter (2006)	-0.008	0.831	Spectroscopic study of 216 stars within 15 pc
33	Ammons et al. (2006)	-0.100	1.000	Only remaining disk sources added that were not available from other catalogs

<sup>†</sup> Metallicities had to be recalculated based on the procedure given in the paper, as on-line data had errors of missing  $\pm$  indexes of metallicities.

**Table 3**

The combined metallicity catalog of 20811 sources. The reference numbers are based on the sequence numbers in Table 2. Only the first 10 lines are displayed, the full table is available online at ApJ or at CDS.

HIP	HD	Simbad	$[\text{Fe}/\text{H}]$	$\sigma_{[\text{Fe}/\text{H}]}$	Refs
HIP000004	HD224707	HD 224707	-0.45	0.10	6
HIP000020	HD224723	HD 224723	-0.25	0.10	6,33
HIP000023	HD224742	HD 224742	-0.26	0.08	6,7,33
HIP000033	HD224743	HD 224743	-0.06	0.10	6,33
HIP000034	HD224758	HR 9078	0.05	0.07	6,7,22,33
HIP000038	HD224752	HD 224752	-0.14	0.10	6,33
HIP000039	HD224763	NLTT 58719	-0.16	0.10	6,33
HIP000042	HD224771	HD 224771	-0.02	0.10	6,33
HIP000050	HD224782	HD 224782	0.44	0.10	6,33
HIP000055	HD224783	HD 224783	0.16	0.10	6,33

In Table 2, we list the metallicity catalogs we merged in sequential order and the conversion factors used. We also note special circumstances with some of the data. Our final merged catalog contains  $[\text{Fe}/\text{H}]$  and  $\sigma_{[\text{Fe}/\text{H}]}$  values for 20811 sources, all in a common system. The sample includes 48 chemically peculiar  $\lambda$  Boötis type stars for which the metallicities are not indicative of the environment they formed in, but of the peculiar surface composition of the star. None of these sources were analyzed in our work, even if they had a disk or upper limit measurement. We present our combined metallicity catalog in Table 3 for future reference.

Outlier metallicities may result from unidentified abundance peculiarities. Therefore, for our analysis we only considered sources with metallicities between  $-0.6 \geq [\text{Fe}/\text{H}] \geq 0.4$ , based on the results of Casagrande et al. (2011) that demonstrate that virtually all stars in the solar neighborhood have metallicities within this range. Our original sample in-

cluded 28 such sources. We also removed 20 sources with  $v \sin(i)$  values above  $200 \text{ km s}^{-1}$ , as such large rotational velocities make it difficult to determine the stellar metallicity accurately (R. Gray, private communication).

One important issue is that the measured stellar abundances may not be representative of the average through the entire stellar volume. Stars without significant envelope convection tend to have strata with varying metal content (e.g., LeBlanc et al. 2009), that can yield an apparent metallicity that differs significantly from the average for that star. The lack of convective mixing can lead to other types of metallicity anomaly, such as the  $\lambda$  Boötis phenomenon, perhaps produced by accretion of relatively small amounts of material onto the stellar surface layer (e.g., Jura 2015). Presumably similar processes at a lower level can produce anomalies below the threshold for identification as a *bona fide*  $\lambda$  Boötis-type star. In fact, a significantly larger scatter in A-star metallicity measurements relative to those for later-types is seen in open clusters (Gebran et al. 2008; Gebran & Monier 2008; Gebran et al. 2010). Debris disk samples generally contain a number of A-stars, in which case the measured abundances against which the disk presence is measured may have large errors and systematic biases. Therefore, we have looked at the possible correlations both for our entire sample, and just for those stars cool enough to have substantial convective outer layers that should produce more homogeneous metallicity behavior. To be conservative, we have divided the nonconvective and convective samples at the A9/F0 transition (Böhm-Vitense 1966; Simon et al. 2002). For similar reasons, metallicity values of early-type stars in nearby moving groups were averaged with the moving group average value.

Another consideration is that debris at detectable levels is largely absent for M-stars (e.g., Heng & Malik 2013), although the incidence of excesses seems to not change significantly down through early K-stars (Sierchio et al. 2014). Therefore, to avoid contaminating any effects with stars with only upper limits regardless of metallicity, we have cut from the sample stars later than K5. The sample trimmed of A-stars and late-type ones is reduced by 127 sources (20 warm detections, 41 warm upper limits, 103 cold detections, 75 cold upper limits). Many of our analyses will be done both for this trimmed sample and for the full sample; we find relatively little difference in the results.

#### 4. ZERO AGING THE SYSTEMS

Debris Disks are in a persistent state of collisional evolution, with the smaller particles eroding away at the larger rocks, producing more dust and more erosion (Wyatt 2008). A quasi steady state is reached (Thébaud et al. 2003; Krivov et al. 2005; Gáspár et al. 2012a), without runaway small dust production, due to the blowout of the smallest  $\mu\text{m}$  size particles in the systems via radiative and corpuscular forces (Burns et al. 1979). Due to the continuous collisional erosion, over time, the disks lose mass and their thermal emission in the mid and/or far-IR fades away (Wyatt 2008; Gáspár et al. 2013). Initially, this process is dominated by evolution from initial conditions set early in the life of the star, probably even by the mass of its protoplanetary disk (Wyatt et al. 2007; Gáspár et al. 2013). The influence of large collisions is transitory and generally minor (Kenyon & Bromley 2005) until the primary evolutionary phase is past, when the incidence of disks drops precipitously (Sierchio et al. 2014). Many of the remaining disks are probably the result of recent and transitory events (Gáspár et al. 2013). This behavior provides an opportunity to take a disk of any age within the slowly-decaying initial phase and use models of its evolution to estimate its characteristics at a young age. That is, it allows de-aging debris disks for an ensemble of stars of different ages to a common age. In this paper, we use our evolutionary collisional cascade model, CODE-M (Gáspár et al. 2012a), to carry out these calculations.

##### 4.1. Procedure

We model the collisional evolution of each individual disk using the collisional cascade code. Apart from the disk radial distance, disk width, disk height, the spectral/emission properties of the host star, and disk mass, all other variables of our models are the same as that of our Reference Model in Gáspár et al. (2012b). The radial distance was determined from the thermal location of the disks, assuming that the emitting dust is in thermal equilibrium and that the stellar radiation is well approximated by the best fitting Kurucz model to the UBVR<sub>I</sub>JHK photometric data of each source. The fitting was done in logarithmic flux space, following filter band-pass corrections. Relatively accurate thermal locations are available for disks observed with *Spitzer* IRS; for all other sources we assumed a standard warm and cold disk thermal location of 190 and 60 K, respectively (Morales et al. 2011; Ballering et al. 2013). The width and height of the disks were set to 10% of the radial distance, while the radiation forces acting on the particles were calculated from the best fitting Kurucz models, assuming astronomical silicate particles (Draine & Lee 1984). Additional numerical and modeling considerations are described in Gáspár et al. (2012a). For the current study, the relative values of the disk parameters

are important, so a consistent set of models is adequate without requiring that the models be correct in an absolute sense (which would, e.g., require consideration of more complex grain compositions).

The modeled evolution of the system flux is fitted to the observed emission using the scaling laws we introduced in Gáspár et al. (2013). As detailed there, since the evolution is always slower than  $t^{-1}$  and the evolutionary tracks scale along  $t^{-1}$  as a function of system mass, there is only a single solution to the scaling of the evolutionary track. This scaling yields the true zero-age system dust mass in units of the original modeled system mass. Once the correct scaling is found, system variables (such as dust mass) can be calculated at any point in time during the evolution of the system.

Modeling of the disks took on average  $\approx 8$  days for each disk, at which point the mid- and/or far-IR flux evolutionary track of the system could be scaled along a  $t^{-1}$  axis in such a way that it intersected the observed system flux, as detailed above. Using a 32 node computer cluster, running the code for all 662 systems took altogether over 15 CPU years.

In Figure 1, we show the process of deaging the systems. Since our initial particle size distribution is slightly shallower than the final steep size distribution that results from a collisional cascade (Gáspár et al. 2012b), the emission of the disks actually increases in the initial phase of the disk evolution while the system is settling into its quasi steady state. This can be seen for some of the lower initial mass systems in Figure 1. Therefore, we define “zero-age” at 1 Myr. The initial conditions of the systems are somewhat uncertain. However, apart from the previously mentioned settling phase, they will not greatly affect the evolution. We verified this by analyzing the results at multiple ages near the “zero-age” point.

We calculated the total system dust mass at these points in time, by integrating the particle size distributions calculated by our numerical code at the corresponding model time and scaling by the factor determined from the flux fits for each system. The distributions are integrated up to 1 mm in radius and the final disk dust masses are divided by the masses of their central stars (in solar units) to place all systems on similar scales. This final step also makes the disk mass metric analogous to metallicity. Due to the many orders of magnitude covered in disk mass space and only a few factors of difference in stellar masses, the normalization by stellar mass did not make a noticeable difference in our final results. In our Figures we plot “reduced masses”, which are the disk dust masses divided by Earth mass and the mass of the central star in solar units ( $M_{\text{reduced}} = M_{\text{dust}}/M_{\oplus}/M_{*}/M_{\odot}$ ). We summarized the warm and cold disk properties in Tables 4 and 5, respectively.

##### 4.2. Application

As shown in Gáspár et al. (2013), the observed fraction of warm debris disks, with excesses 10% above the stellar photosphere, decay to only a few percent for sources older than  $\sim 500$  Myr. This trend is independent of the spectral-type of the host star. Since our code models quasi-steady state collisional cascades, we only include sources with ages up to 500 Myr in our correlation analysis, as many sources that are older are likely experiencing a late-stage stochastic event. With this cut, our warm disk sample has 199 sources, 188 observed by MIPS/*Spitzer* at 24  $\mu\text{m}$  (63 detections and 125 upper limits) and 11 observed only by WISE at 22  $\mu\text{m}$  (only detections).

Unlike the warm disks, cold debris disks can evolve in a quasi-steady state collisional cascade well up to 5 Gyr

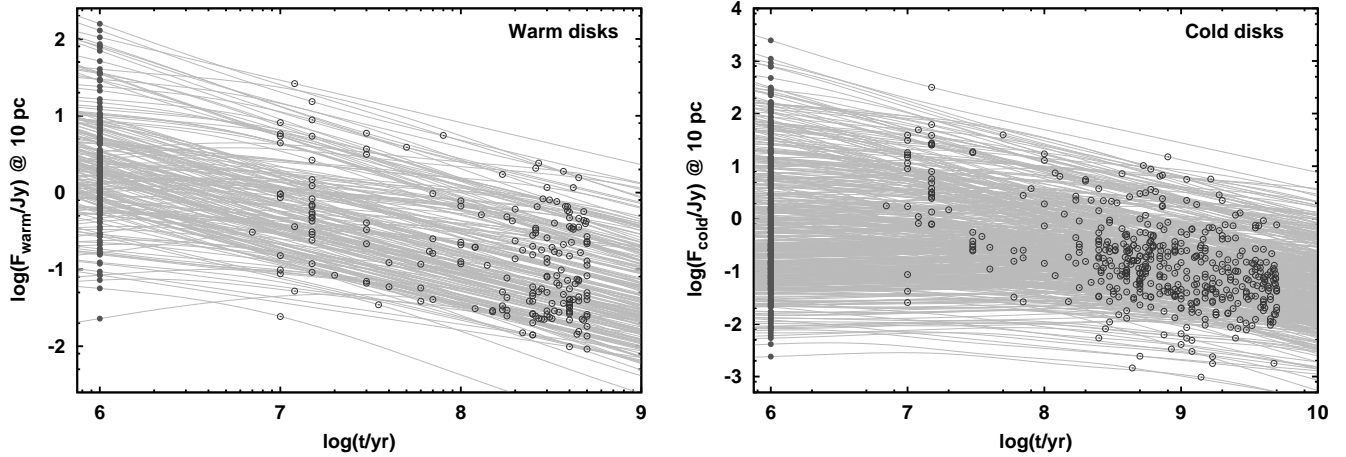


**Figure 1.** The process of de-aging the disk fluxes is shown for the warm disk sample (*left panel*) and cold disk sample (*right panel*). Since the disk and stellar parameters vary from one system to another, each evolution curve had to be calculated for each individual system separately. Once the mass scaling of each curve is found that allows the curve to intersect the observed photometry, the mass can be traced to any point in the evolution. The observed photometry points are shown with empty circles, while the traced points at 1 Myr are shown with filled circles. The disk fluxes (photosphere subtracted) are scaled to a hypothetical source distance of 10 pc.

(Gáspár et al. 2013; Sierchio et al. 2014), therefore we made an age cut at 5 Gyr in the sample when analyzing a possible correlation between the cold disk dust mass and host star metallicity. Our cold disk sample has 463 sources (148 detections and 315 upper limits), observed by MIPS/*Spitzer* at  $70\ \mu\text{m}$  and/or by PACS/*Herschel* at  $100\ \mu\text{m}$ . If a source was observed at both bands, we averaged the disk dust mass predicted for each band.

## 5. RESULTS

### 5.1. Confirming Previous Evidence for a Metallicity Dependence (Maldonado et al. 2012)

Maldonado et al. (2012) merged multiple sets of data on debris disk excesses of solar-like (F5 - K2/3) stars and compared the distribution of metallicities for those with detected disks and those without. For their full sample, the Kolmogorov-Smirnov (KS) test indicated a probability of 9% that the two samples were drawn from the same parent sample (although the smaller sample based only on their own metallicity measurements did not show such an effect (Maldonado et al. 2015)). The Maldonado et al. (2012) study was based on 107 disk detections and 145 non-detections around solar-like stars, mixing warm and cold disks (although most of their disks were detected at *Spitzer*-MIPS  $70\ \mu\text{m}$ ). All other studies (excepting Maldonado et al. (2015)) were based on less than 40 sources, so it is not surprising that this hint is not apparent in them.

To test this result, we did an analysis comparing detected with undetected disks for the far infrared/cold disks<sup>4</sup> based on our trimmed sample including spectral types of F0 - K5 (compared with F5 - K2/3 for Maldonado et al. (2012); in addition to the slightly broader range in spectral type, our sample has systems removed that are sufficiently old that debris disks are unexpected as a product of quiescent evolution). Since we reconciled systematic differences in metallicity determinations in the process of assembling all the relevant [Fe/H] measurements, our sample is equivalent in this sense to the *homogeneous* sample of Maldonado et al. (2012). The debris disk discriminator “detected” vs. “nondetected” does not

yield a physically well-defined boundary, since it depends on the observational circumstances as well as the character of the disk. We therefore considered thresholds in terms of our de-aged reduced disk masses. For each threshold, we counted only the detected disk masses above the fiducial value (not the upper limits) for one sample, and counted all detections and upper limits below the threshold for the other sample. The useful range of thresholds runs from  $\log(M_{\text{reduced}}) = -2$  to  $\log(M_{\text{reduced}}) = -4$ ; above this range there are too few detections and below it too few detections and upper limits for a meaningful study of metallicity effects.

Figure 2 shows the results - for completeness, for both the full and trimmed (F0 - K5) cold disk sample. For every threshold, the incremental number of systems with increasing [Fe/H] has very similar behavior. Above [Fe/H] =  $-0.1$ , the systems below and above the dust mass dividing line have very similar distributions indicating that the majority of undetected stars are similar to those with detected disks, but presumably are undetected because of less rich planetesimal systems or less vigorous dynamical stirring of those systems (the latter probably independent of metallicity). Below [Fe/H] =  $-0.1$ , the distributions of detected and undetected systems are dramatically different, with a strong trend toward low metallicity systems not having massive debris disks. This result therefore confirms and expands the finding by Maldonado et al. (2012) of a deficit of debris-disk-bearing stars over the range  $-0.5 \leq [\text{Fe}/\text{H}] \leq -0.2$ . The K-S test of the trimmed sample with a cutoff threshold of  $\log(M_{\text{reduced}}) = -4$  yields  $p_{\text{KS}} \sim 0.15$ , in agreement with the (Maldonado et al. 2012) result. We also analyzed the samples with the Anderson-Darling (AD) statistic (Scholz & Stephens 1987), which gave a  $p_{\text{AD}} \sim 0.09$ . The nominal significance of the difference in distributions depends on the way the tested hypothesis is posed: 1.) if, as above and by Maldonado et al. (2012), it is whether the global distributions differ, the result is a strong hint of a correlation; however, 2.) if the question is whether there is a tendency against significant debris systems for stars with less than solar [Fe/H], the statistical significance of the difference (e.g., comparing distributions for [Fe/H] < 0) is greater.

<sup>4</sup> The warm disk sample shows similar behavior but at lower weight.

**Table 4**

The observed and de-aged parameters of the warm disk sources at  $t = 1$  Myr and at the actual ages. Dust masses are calculated for particles ranging in size from the blowout limit to 1 mm in radius. The fluxes displayed are for the disks only (photosphere subtracted) and calculated for the system being @ 10 pc to allow for comparison. The type denotes either 22  $\mu\text{m}$  WISE detection, 24  $\mu\text{m}$  Spitzer detection, or 24  $\mu\text{m}$  Spitzer Upper limit. Only the first 10 lines are displayed, the full table is available online at ApJ or at CDS.

HIP	Name HD	$T_{\text{warm}}$ (K)	$R_{\text{warm}}$ (AU)	$F_{\text{warm}}$ (mJy)@10 pc	$F_{\text{warm}}(1)$	$M_{\text{dust}}$ ( $\log(M_{\text{dust}}/M_{\oplus})$ )	$M_{\text{dust}}(1)$ ( $\log(M_{\text{dust}}/M_{\oplus})$ )	Type
HIP000490	HD000105	190.00	2.44	50.8	1988.1	-6.369	-4.777	U
HIP000544	HD000166	126.40	3.79	38.6	1963.1	-5.920	-4.214	S
HIP000560	HD000203	190.00	4.40	52.1	72.5	-6.248	-6.092	U
HIP000682	HD000377	119.30	5.90	177.6	9525.3	-5.079	-3.350	S
HIP001134	HD000984	190.00	3.14	59.1	3392.0	-6.257	-4.499	U
HIP001292	HD001237	190.00	1.72	25.7	852.3	-6.725	-5.206	U
HIP001473	HD001404	132.90	20.30	461.7	1074.9	-4.285	-3.870	S
HIP001481	HD001466	216.60	1.96	235.1	4381.4	-5.881	-4.611	S
HIP001803	HD001835	190.00	2.19	74.7	2741.8	-6.215	-4.650	U
HIP002578	HD003003	194.40	8.13	3136.1	35296.6	-4.285	-3.234	S

**Table 5**

The observed and de-aged parameters of the cold disk sources at  $t = 1$  Myr and at the actual ages. Dust masses are calculated for particles ranging in size from the blowout limit to 1 mm in radius. Where dust masses could be calculated from both 70 and 100  $\mu\text{m}$  observations, the dust masses were averaged. The fluxes displayed are for the disks only (photosphere subtracted) and calculated for the system being @ 10 pc to allow for comparison. The type denotes either a detection at 70 or 100  $\mu\text{m}$  (**70D** or **100D**) or an upper limit (**70U** or **100U**). Only the first 10 lines are displayed, the full table is available online at ApJ or at CDS.

HIP	Name HD	$T_{\text{cold}}$ (K)	$R_{\text{cold}}$ (AU)	$F_{70}$ (mJy)@10 pc	$F_{70}(1)$	$F_{100}$ (mJy)@10 pc	$F_{100}(1)$	$M_{\text{dust}}$ ( $\log(M_{\text{dust}}/M_{\oplus})$ )	$M_{\text{dust}}(1)$ ( $\log(M_{\text{dust}}/M_{\oplus})$ )	Type
HIP000490	HD000105	47.84	33.70	2263.236	11950.800	-	-	-2.501	-1.779	70D
HIP000544	HD000166	49.92	21.38	125.698	256.054	87.705	160.267	-3.907	-3.620	70D,100D
HIP000560	HD000203	128.70	9.63	1097.957	1983.503	-	-	-3.962	-3.705	70D
HIP000682	HD000377	43.89	37.44	2253.957	11157.030	-	-	-2.380	-1.684	70D
HIP000910	HD000693	60.00	34.62	38.627	58.293	14.727	20.442	-4.688	-4.531	70D,100D
HIP000950	HD000739	60.00	34.50	44.455	69.758	161.114	534.236	-4.133	-3.766	70U,100U
HIP001031	HD000870	50.16	18.93	68.318	4293.173	-	-	-4.164	-2.366	70D
HIP001134	HD000984	60.00	28.93	371.446	742.581	-	-	-3.567	-3.262	70U
HIP001292	HD001237	60.00	15.80	26.943	45.663	31.046	62.718	-4.659	-4.390	70U,100U
HIP001368	-	36.84	15.55	33.272	113.487	87.006	368.355	-3.824	-3.244	70D,100D

### 5.2. Metallicity effects in our warm and cold samples

In Figure 3, we show the same distribution functions for the warm disk sample. At a reduced mass cut of  $\log(M_{\text{reduced}}) = -4$  a similar discrepancy can be seen between the distributions as for the cold disk systems, with  $p_{KS} \sim 0.07$ . The AD statistic gave a higher  $p_{AD} \sim 0.2$  value for the warm sample, likely do to the low number of sources (14) in one of the samples. Finally, we repeated this test for cold disks around stars older than 0.5 Gyr. Since we required an age below this value for the warm disks, this is a completely independent sample. The results, exhibited in Figure 4, again demonstrate, with  $p_{KS} \sim 0.11$  ( $p_{AD} \sim 0.08$ ), an absence of disks with  $[\text{Fe}/\text{H}] \leq -0.2$ . The very similar behavior in *both* Figures 3 and 4 supports that the lack of disks at low metallicity is a significant trend.

### 5.3. Survival Analysis

The previous section found evidence for an effect in terms of the metallicity as a function of the disk properties. We now probe in the orthogonal sense, i.e., the disk properties as a function of the metallicity. We divide each of the warm and cold samples into three equal-sized bins in metallicity. For the warm sample, the demarcations are at  $[\text{Fe}/\text{H}] = -0.085$  and 0.034, with 66 disks in each bin, including the censored data (upper limits). This roughly defined a metal poor, a solar metallicity, and a metal rich group. For the cold disk sample, the demarcations were at almost the same values,  $[\text{Fe}/\text{H}] = -0.09$  and 0.028, with 154 disks in each group, including censored data (upper limits). We will investigate the

mass distribution of the disks in each of these bins.

The Kaplan-Meier (K-M) survival estimator (Kaplan & Meier 1958) provides a systematic method for doing so. Originally developed for biological studies (hence its slightly inappropriate name), survival analysis has been adopted for astronomical data analysis (e.g., Feigelson & Nelson 1985), where it is useful for randomly picked datasets. We used the statistical routine `survfit` in the NADA package of R to calculate the K-M survival estimate with increasing dust mass within each of these groups for the systems at their current ages and the de-aged 1 Myr old total dust mass distributions. The routine also calculates the 95% confidence intervals of the survival estimates.

We show the disk dust mass vs. metallicity distribution of the lower and higher metallicity bins for the warm disk sample and the survival functions of the sources in mass space at the current ages and for the de-aged results in Figure 5 (the intermediate metallicity bin generally falls near the high metallicity case). The data point sizes in the distribution plots are proportional to the inverse of their metallicity errors to guide the eye in weighting each point. The top row of the figure shows the plots for the full, while the bottom is for the trimmed F0-K5 spectral-type sample. There is a hint of a difference with metallicity prior to de-aging the systems. Applied to the de-aged results, this test shows that at 1 Myr, near the time of their formation, there is perhaps a modest trend with metallicity for the least massive disks, but a significant trend develops with increasing mass. It is especially noteworthy that the

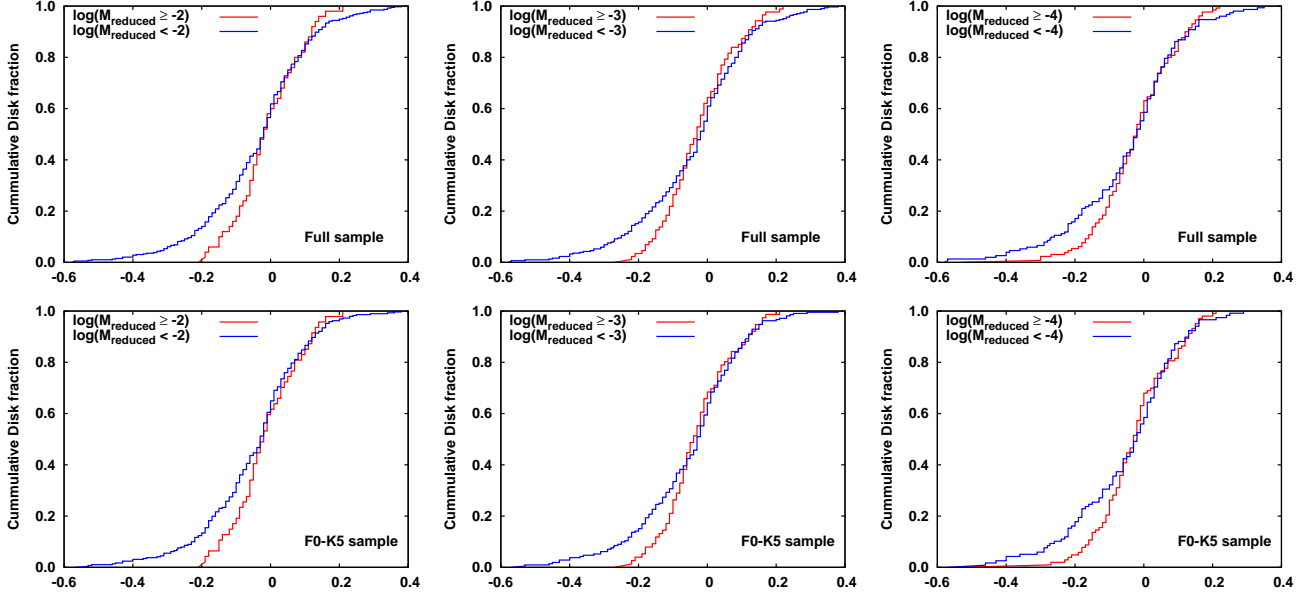


**Figure 2.** The cumulative disk fraction of the cold disk sample at various  $M_{\text{reduced}}$  values for both the full and F0-K5 subsample.

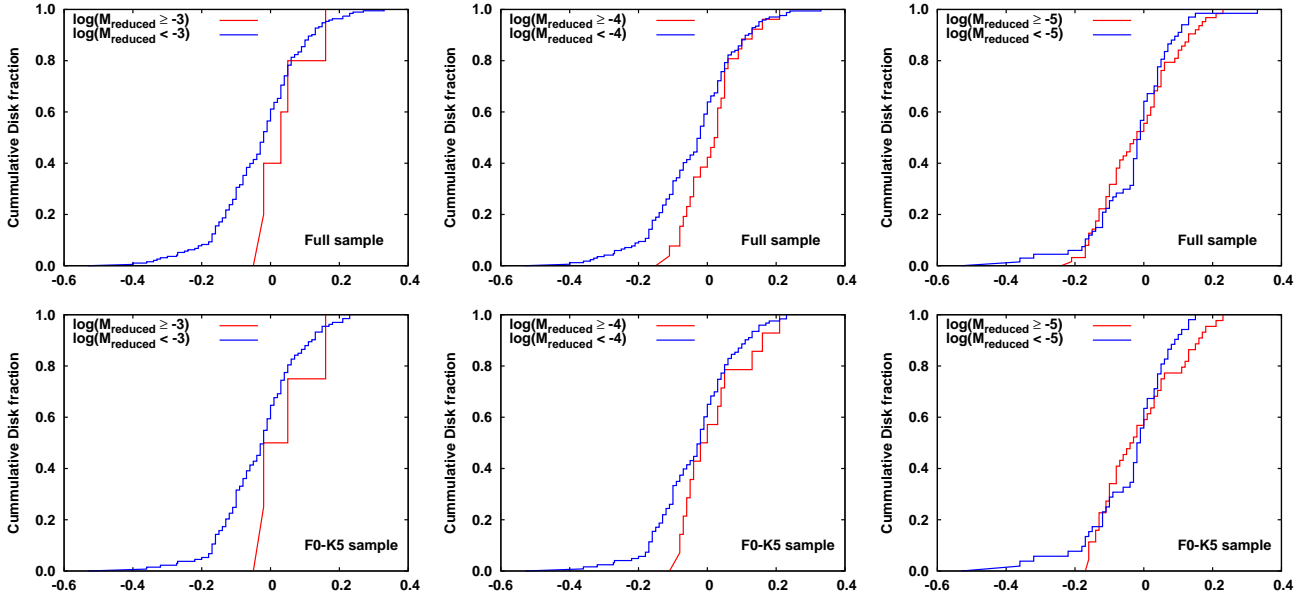


**Figure 3.** The cumulative disk fraction of the warm disk sample at various  $M_{\text{reduced}}$  values for both the full and F0-K5 subsample.

highest mass system in the metal poor sample has a reduced mass of  $\log(M_{\text{reduced}}) = -3.5$ , while there are 4 sources more massive than this value in each of the higher metallicity bins. This behavior suggests a metallicity-dependent upper limit to the disk masses, which seems plausible from visible inspection of the left plot.

We show the disk dust mass vs. metallicity distribution of the three metallicity bins in the cold sample at both ages and the survival functions of the sources in dust mass space in Figure 6. The survival functions agree with each other within their 95% confidence intervals for all the bins, although that for the low metallicity bin tends to fall below that for the high metallicity one for the higher-mass disks. There may be a trend at the  $\sim 1\sigma$  level for low metallicity systems not to have

massive disks, but this result is by itself not statistically significant.

#### 5.4. Form of the Disk Mass vs. $[Fe/H]$ Relation

We have tried to extract more information about the relationship between disk mass and stellar metallicity by carrying out linear regression on the low and high metallicity portions of our sample. There are significant challenges in doing so: the dataset we are analyzing has errors in both variables (metallicity and system dust mass) and also has censoring (upper limits on the dust mass) for some of the data. The errors in metallicity were derived when we merged the catalogs (as described in section 3), while the errors in the de-aged dust masses were calculated based on the photometry errors, with



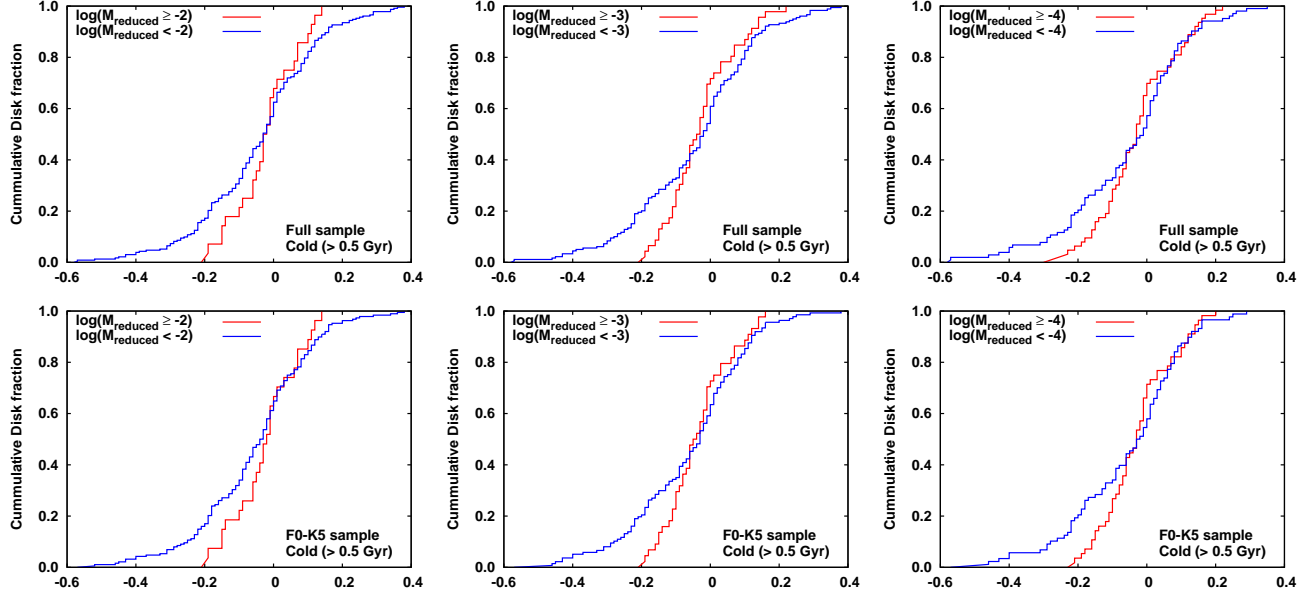


**Figure 4.** The cumulative disk fraction of the cold disk sample at various  $M_{\text{reduced}}$  values for both the full and F0-K5 subsample, including only sources that are older than 0.5 Gyr.

de-aging performed using the flux values at the error boundaries as well. An ideal method would include upper limits as censored data, as well as allowing for these sources of error<sup>5</sup>.

We evaluated two linear regression techniques for this purpose, the Gaussian mixed Bayesian (GmB) method (Kelly 2007) and the Akritas-Theil-Sen (ATS) estimator (Akritas et al. 1995). Datasets with errors in both variables and with censoring have been shown to be reasonably well fit with GmB linear regression methods. As a first approach, we fit our data using said method with the `linmix_err` algorithm developed by Kelly (2007). Unfortunately, both the metallicity and de-aged dust masses have significant heteroscedastic errors and the metallicity vs. dust mass plots show large scatter with outliers and censoring. The GmB regression method is skewed by outliers, as it assumes a Gaussian error distribution for  $(Y|X)$ . However, our dataset has a non-uniform and non-Gaussian error distribution, and the upper limits in our sample do not reflect simple Gaussian errors due to the differing source distances. These issues were apparent upon inspection of the GmB fits, so we decided this approach was not applicable in our situation.

The Theil-Sen (Theil 1950; Sen 1968) regression slope estimator modified by Akritas et al. (1995), is able to filter outliers and also use censored data. The classic Theil-Sen estimator gives the regression slope as the median slope of all pairs of sample points. This algorithm was modified by Akritas et al. (1995) to allow for censoring. To take into account data errors we bootstrapped using the errors in the data, generating 1000 random sets with the data distributed based on the parameter errors. We then fitted the distributions with the `cenken` ATS routine in R, which finds the regression slope via iterations, with the solution being the slope that yields a Kendall  $\tau$  of 0 when removing the values of the test-slope from the data. Therefore, any non-zero regression slope

<sup>5</sup> Since age errors were not readily available, we did not take into account possible errors in the system variables resulting from the age uncertainties. Since the errors in metallicity are dominant in the scatter plot, including errors from age uncertainties would not have made a significant difference in our conclusions.

also means a non-zero value of the Kendall  $\tau$ .

We divided the warm and cold samples at  $[\text{Fe}/\text{H}] = 0$  and used the ATS estimator to fit slopes to each metallicity bin. The results are in Figure 7; for simplicity, we only show them for the full spectral sample de-aged to 1 Myr. The narrow range in metallicity results in large errors in the slopes. For three cases, warm disks with  $[\text{Fe}/\text{H}] < 0$  and  $> 0$  and cold disks with  $[\text{Fe}/\text{H}] > 0$ , the slopes are close to zero but the 95% probability error ranges allow a correlation as strong as disk mass going as the square of the metallicity. For the cold disks and  $[\text{Fe}/\text{H}] < 0$ , a significant slope is indicated in the expected direction, i.e., disks of significant mass are uncommon around low metallicity stars.

## 6. CONCLUSIONS

Since their early discovery (Aumann et al. 1984; Smith & Terrile 1984; Backman & Paresce 1993), debris disks have always been thought of as signposts of planetary systems. However, there are few examples where direct connections between debris disk properties and those of exoplanetary systems have been established. In this paper we revisited this conundrum.

We gathered *Spitzer* and *Herschel* data on 199 warm disks (of which 125 only have upper limits) and 463 cold disks (of which 315 only have upper limits) around 478 hosts. Through the merging of 33 individual spectral catalogs, we also collected metallicity data for these systems. Using our collisional cascade model (Gáspár et al. 2012a), we then “de-aged” the systems, yielding dust masses for the systems at the time of their formation. We found multiple indications that massive debris disks are uncommon at low stellar metallicity (e.g.,  $[\text{Fe}/\text{H}] < -0.2$ ). Although not all of these indicators individually are at a high level of statistical significance, their combination points to a real avoidance by debris disks of low metallicity environments.

These results are in qualitative agreement with the planet-metallicity correlation (Gonzalez 1997; Fischer & Valenti 2005) and the core-accretion formation model (Mizuno 1980; Ikoma et al. 2000) (where the heavier elements aggregate into

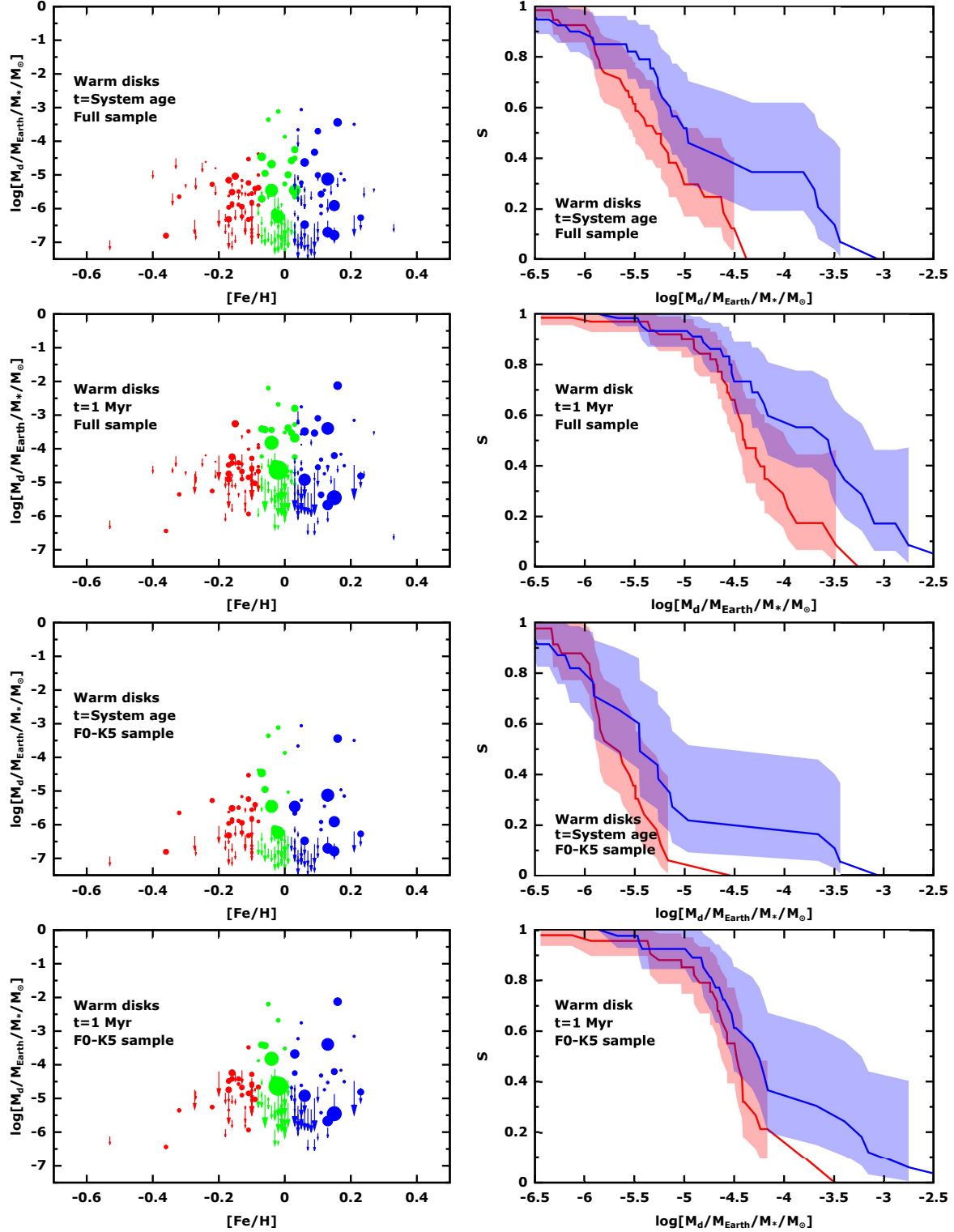


**Figure 5.** Survival analysis of the disk dust mass distributions for the warm debris disks, with the samples divided into three metallicity bins with equal numbers of members. The first two rows show plots for the full sample, while the last two rows show plots for the F0-K5 subsample. In the left plots, the sizes of the points are inversely in proportion to their errors - the largest points have the smallest errors - to guide the eye in weighting the points. The error bands in the KM analyses to the right give a 95% confidence interval at each disk dust mass. For clarity, we only show the KM functions of the low and high metallicity bins; the KM function of the solar-metallicity bin roughly agrees with the KM function of the higher metallicity one. At 1 Myr, the metal-poor bin has a significantly steeper survival function, with lower mass disks than the solar and metal-rich groups. This difference shows that the metal poor bin is drawn from a different parent disk dust mass distribution than the metal rich bin. The difference grows with increasing dust mass, consistent with the presence of a metallicity-dependent upper envelope to the dust mass.

dust and further on to planetesimals) and the type II migration models of close orbit giant planets (Goldreich & Tremaine 1980; Armitage 2007). Fischer & Valenti (2005) found that the planet-metallicity correlation is a result of system initial conditions rather than acquired via accretion, i.e. planetary systems with close orbit giant planets are more likely to form from molecular clouds with higher initial metal content. Debris disks generally bound the regions of giant planet formation, with the warm components defining the inner and the cold components the outer edges. Our finding therefore corresponds roughly with the strong dependence of the incidence of giant planets on metallicity (e.g., Fischer & Valenti 2005; Johnson et al. 2010; Wang & Fischer 2015).

Support for this work was provided by NASA through Contract Number 1255094 issued by JPL/Caltech. This research has made use of the SIMBAD database, operated at CDS, Strasbourg, France.

## REFERENCES

- Acke, B., et al. 2012, *A&A*, 540, A125
- Akratis, M. G., Murphy, S. A., & LaValley, M. P. 1995, *J. Amer. Statist. Assoc.*, 90, 170
- Ammons, S. M., Robinson, S. E., Strader, J., Laughlin, G., Fischer, D., & Wolf, A. 2006, *ApJ*, 638, 1004
- Andrievsky, S. M. 1998, *A&A*, 334, 139
- Armitage, P. J. 2007, *ApJ*, 665, 1381
- Aumann, H. H., et al. 1984, *ApJ*, 278, L23
- Backman, D. E., & Paresce, F. 1993, in *Protostars and Planets III*, ed. E. H. Levy & J. I. Lunine, 1253–1304
- Bailey, V., et al. 2014, *ApJ*, 780, L4
- Ballerie, N. P., Rieke, G. H., Su, K. Y. L., & Montiel, E. 2013, *ArXiv e-prints*
- Beichman, C. A., et al. 2006, *ApJ*, 652, 1674
- Bennett, D. P., Anderson, J., Bond, I. A., Udalski, A., & Gould, A. 2006, *ApJ*, 647, L171
- Böhm-Vitense, E. 1966, *Transactions of the International Astronomical Union, Series B*, 12, 547
- Bond, J. C., Tinney, C. G., Butler, R. P., Jones, H. R. A., Marcy, G. W., Penny, A. J., & Carter, B. D. 2006, *MNRAS*, 370, 163
- Borucki, W. J., et al. 2010, *Science*, 327, 977
- Boss, A. P. 2002, *ApJ*, 567, L149
- Bryden, G., et al. 2006, *ApJ*, 636, 1098
- Buchhave, L. A., et al. 2014, *Nature*, 509, 593
- Burns, J. A., Lamy, P. L., & Soter, S. 1979, *Icarus*, 40, 1
- Cai, K., Durisen, R. H., Michael, S., Boley, A. C., Mejía, A. C., Pickett, M. K., & D'Alessio, P. 2006, *ApJ*, 636, L149
- Casagrande, L., Schönrich, R., Asplund, M., Cassisi, S., Ramírez, I., Meléndez, J., Bensby, T., & Feltzing, S. 2011, *A&A*, 530, A138
- Chen, C. H., Mittal, T., Kuchner, M., Forrest, W. J., Lisse, C. M., Manoj, P., Sargent, B. A., & Watson, D. M. 2014, *ApJS*, 211, 25
- Chiang, E., Kite, E., Kalas, P., Graham, J. R., & Clampin, M. 2009, *ApJ*, 693, 734
- Cossou, C., Raymond, S. N., Hersant, F., & Pierens, A. 2014, *A&A*, 569, A56
- Cruz-Saenz de Miera, F., Chavez, M., Bertone, E., & Vega, O. 2014, *MNRAS*, 437, 391
- Currie, T., Daemgen, S., Debes, J., Lafreniere, D., Itoh, Y., Jayawardhana, R., Ratzka, T., & Correia, S. 2014, *ApJ*, 780, L30
- Draine, B. T., & Lee, H. M. 1984, *ApJ*, 285, 89
- Eiroa, C., et al. 2013, *A&A*, 555, A11
- Ersparmer, D., & North, P. 2003, *A&A*, 398, 1121
- Favata, F., Micela, G., & Sciortino, S. 1997, *A&A*, 323, 809
- Feigelson, E. D., & Nelson, P. I. 1985, *ApJ*, 293, 192
- Fischer, D. A., & Valenti, J. 2005, *ApJ*, 622, 1102
- Fuhrmann, K. 2008, *MNRAS*, 384, 173
- Gammie, C. F. 2001, *ApJ*, 553, 174
- Garaud, P. 2011, *ApJ*, 728, L30
- Gáspár, A., Psaltis, D., Özel, F., Rieke, G. H., & Cooney, A. 2012a, *ApJ*, 749, 14
- Gáspár, A., Psaltis, D., Rieke, G. H., & Özel, F. 2012b, *ApJ*, 754, 74
- Gáspár, A., Rieke, G. H., & Balog, Z. 2013, *ApJ*, 768, 25
- Gebran, M., & Monier, R. 2008, *A&A*, 483, 567
- Gebran, M., Monier, R., & Richard, O. 2008, *A&A*, 479, 189
- Gebran, M., Vick, M., Monier, R., & Fossati, L. 2010, *A&A*, 523, A71
- Gerbaldi, M., Faraggiana, R., & Caffau, E. 2007, *A&A*, 472, 241
- Goldreich, P., & Tremaine, S. 1980, *ApJ*, 241, 425
- Gonzalez, G. 1997, *MNRAS*, 285, 403
- Gray, R. O., Corbally, C. J., Garrison, R. F., McFadden, M. T., Bubar, E. J., McGahee, C. E., O'Donoghue, A. A., & Knox, E. R. 2006, *AJ*, 132, 161
- Gray, R. O., Corbally, C. J., Garrison, R. F., McFadden, M. T., & Robinson, P. E. 2003, *AJ*, 126, 2048
- Greaves, J. S., Fischer, D. A., & Wyatt, M. C. 2006, *MNRAS*, 366, 283
- Guillout, P., et al. 2009, *A&A*, 504, 829
- Heng, K., & Malik, M. 2013, *MNRAS*, 432, 2562
- Holmberg, J., Nordström, B., & Andersen, J. 2009, *A&A*, 501, 941
- Ikoma, M., Nakazawa, K., & Emori, H. 2000, *ApJ*, 537, 1013
- Jenkins, J. S., Jones, H. R. A., Pavlenko, Y., Pinfield, D. J., Barnes, J. R., & Lyubchik, Y. 2008, *A&A*, 485, 571
- Jenkins, J. S., Ramsey, L. W., Jones, H. R. A., Pavlenko, Y., Gallardo, J., Barnes, J. R., & Pinfield, D. J. 2009, *ApJ*, 704, 975
- Johansen, A., Youdin, A., & Mac Low, M.-M. 2009, *ApJ*, 704, L75
- Johnson, B. C., et al. 2012, *ApJ*, 761, 45
- Johnson, J. A., Aller, K. M., Howard, A. W., & Crepp, J. R. 2010, *PASP*, 122, 905
- Johnson, J. L., & Li, H. 2012, *ApJ*, 751, 81
- Jura, M. 2015, *AJ*, 150, 166
- Kalas, P., et al. 2008, *Science*, 322, 1345
- Kaplan, E. L., & Meier, P. 1958, *Journal of the American Statistical Association*, 53, 457
- Katz, D., Soubiran, C., Cayrel, R., Barbay, B., Friel, E., Bienaymé, O., & Perrin, M.-N. 2011, *A&A*, 525, A90
- Kelly, B. C. 2007, *ApJ*, 665, 1489
- Kennedy, G. M., & Wyatt, M. C. 2014, *MNRAS*, 444, 3164
- Kenyon, S. J., & Bromley, B. C. 2005, *AJ*, 130, 269
- Koleva, M., & Vazdekis, A. 2012, *A&A*, 538, A143
- Kraus, A. L., Ireland, M. J., Cieza, L. A., Hinkley, S., Dupuy, T. J., Bowler, B. P., & Liu, M. C. 2014, *ApJ*, 781, 20
- Krivov, A. V., Sremčević, M., & Spahn, F. 2005, *Icarus*, 174, 105
- Kunzli, M., & North, P. 1998, *A&A*, 330, 651
- Lagrange, A.-M., et al. 2010, *Science*, 329, 57
- LeBlanc, F., Monin, D., Hui-Bon-Hoa, A., & Hauschildt, P. H. 2009, *A&A*, 495, 937
- Lemke, M. 1989, *A&A*, 225, 125
- Luck, R. E., & Heiter, U. 2005, *AJ*, 129, 1063
- Luck, R. E., & Heiter, U. 2006, *AJ*, 131, 3069
- Maldonado, J., Eiroa, C., Villaver, E., Montesinos, B., & Mora, A. 2012, *A&A*, 541, A40
- Maldonado, J., Eiroa, C., Villaver, E., Montesinos, B., & Mora, A. 2015, *ArXiv e-prints*
- Malhotra, R. 2015, *ApJ*, 808, 71
- Mamajek, E. E., & Hillenbrand, L. A. 2008, *ApJ*, 687, 1264
- Marois, C., Macintosh, B., Barman, T., Zuckerman, B., Song, I., Patience, J., Lafrenière, D., & Doyon, R. 2008, *Science*, 322, 1348
- Marshall, J. P., et al. 2014, *A&A*, 565, A15
- Mayor, M., et al. 2009, *A&A*, 493, 639
- Meng, H. Y. A., et al. 2014, *Science*, 345, 1032
- Meru, F., & Bate, M. R. 2010, *MNRAS*, 406, 2279
- Mizuno, H. 1980, *Progress of Theoretical Physics*, 64, 544
- Moór, A., et al. 2013, *ArXiv e-prints*
- Morales, F. Y., Rieke, G. H., Werner, M. W., Bryden, G., Stapelfeldt, K. R., & Su, K. Y. L. 2011, *ApJ*, 730, L29
- Moro-Martín, A., et al. 2015, *ApJ*, 801, 143
- Nayakshin, S. 2015, *MNRAS*, 448, L25
- Nordström, B., et al. 2004, *A&A*, 418, 989
- Panić, O., et al. 2013, *MNRAS*, 435, 1037
- Patel, R. I., Metchev, S. A., & Heinze, A. 2014, *ApJS*, 212, 10
- Paulson, D. B., & Yelda, S. 2006, *PASP*, 118, 706
- Paunzen, E., et al. 2002, *A&A*, 392, 515
- Philip, A. D., & Egret, D. 1980, *A&AS*, 40, 199
- Robinson, S. E., Ammons, S. M., Kretke, K. A., Strader, J., Wertheimer, J. G., Fischer, D. A., & Laughlin, G. 2007, *ApJS*, 169, 430
- Rodigas, T. J., Malhotra, R., & Hinz, P. M. 2014, *ApJ*, 780, 65
- Saffie, C., Gómez, M., Pintado, O., & González, E. 2008, *A&A*, 490, 297
- Schmitt, J. H. M. M., Fleming, T. A., & Giampapa, M. S. 1995, *ApJ*, 450, 392
- Scholz, F. W., & Stephens, M. A. 1987, *Journal of the American Statistical Association*, 82, pp. 918

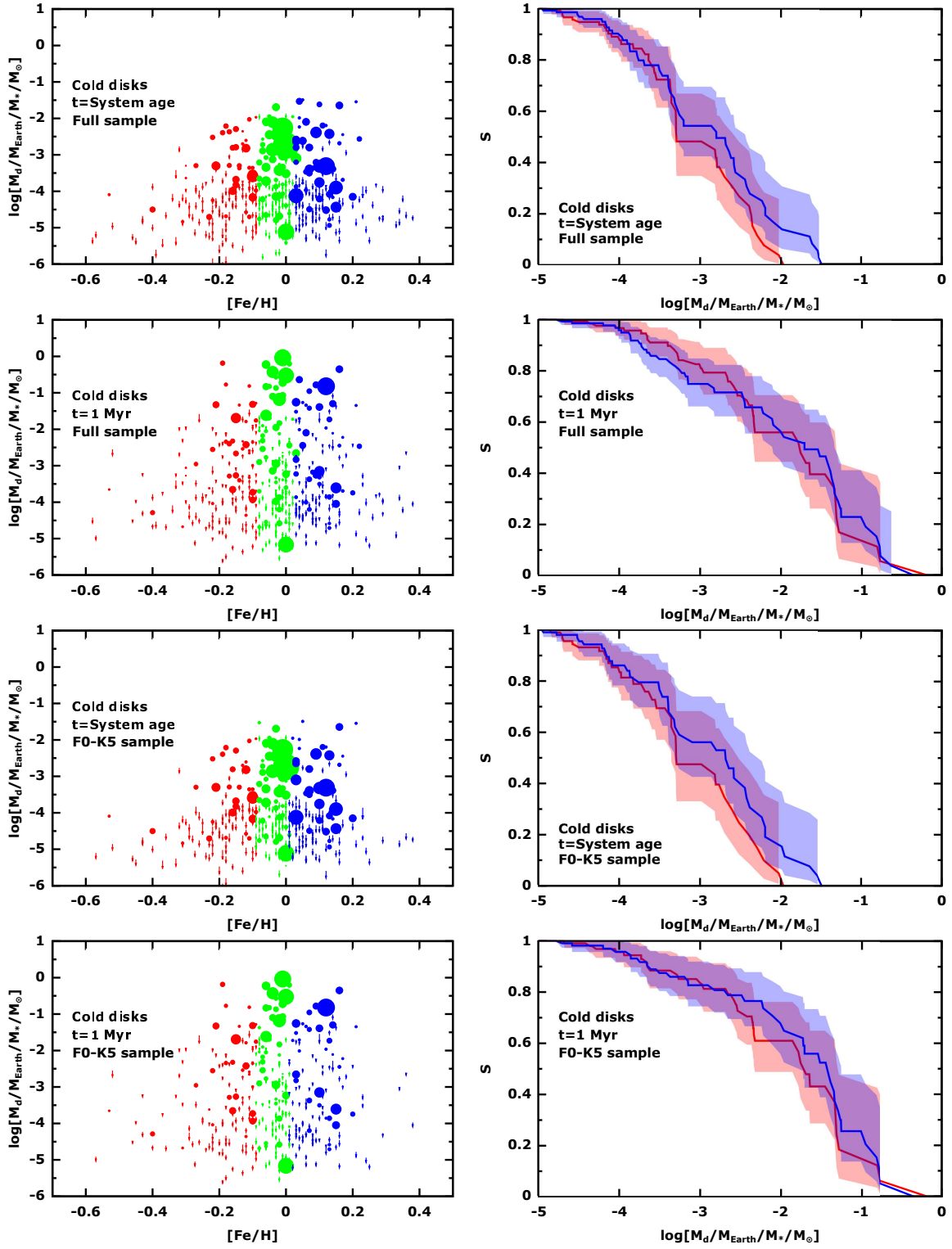


**Figure 6.** Survival analysis of the disk dust mass distributions for the cold debris disks, with the samples divided into three metallicity bins with equal numbers of members. The first two rows show plots for the full sample, while the last two rows show plots for the F0-K5 subsample. In the left plots, the sizes of the points are inversely in proportion to their errors - the largest points have the smallest errors - to guide the eye in weighting the points. The error bands in the KM analyses to the right give a 95% confidence interval at each disk dust mass. For clarity, we only show the KM functions of the low and high metallicity bins; the KM function of the solar-metallicity bin roughly agrees with the KM function of the higher metallicity one.

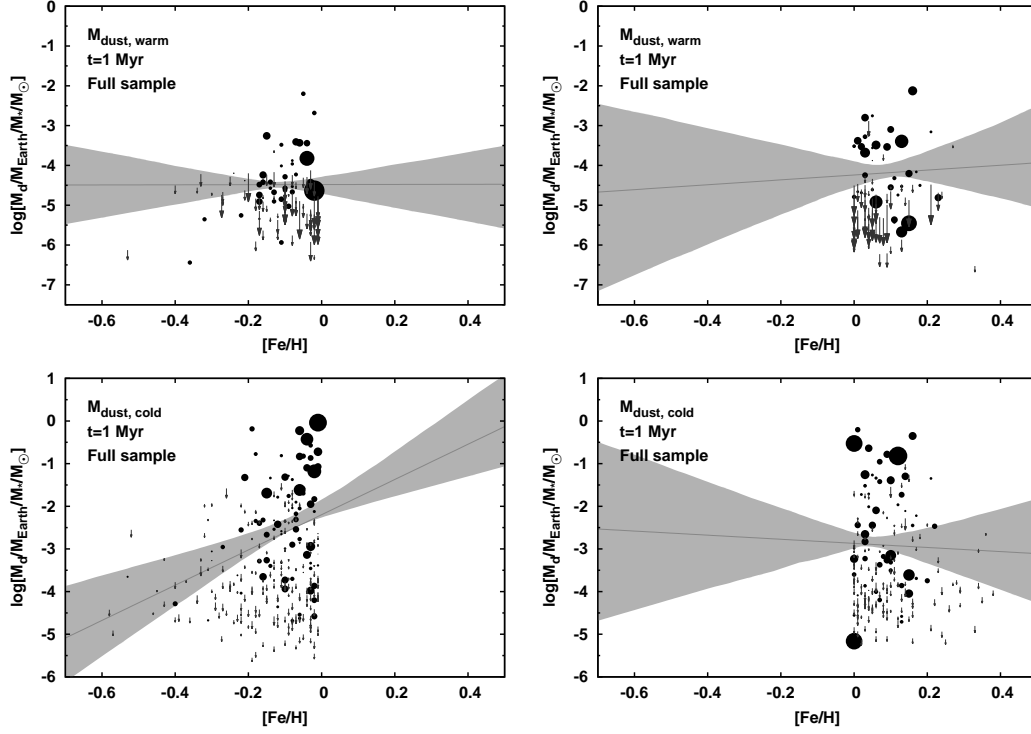


**Figure 7.** Linear regression fits with the warm and cold disk samples divided into low and high metallicity bins at  $[\text{Fe}/\text{H}] = 0$ . The best ATS fit is shown as a line, with the 95% confidence limits in grey. The top row is for the warm systems, the bottom row for cold ones. For simplicity we only show the results for the full disk sample, de-aged to 1 Myr. The point and arrow (upper limits) sizes are inversely proportional to measurement errors, which are generally dominated by errors in metallicity. That is, the points with smaller errors are plotted with larger symbols.

Schuster, W. J., & Nissen, P. E. 1989, *A&A*, 221, 65  
 Sen, P. K. 1968, *J. Amer. Statist. Assoc.*, 63, 1379  
 Sierchio, J. M., Rieke, G. H., Su, K. Y. L., & Gáspár, A. 2014, *ApJ*, 785, 33  
 Simon, T., Ayres, T. R., Redfield, S., & Linsky, J. L. 2002, *ApJ*, 579, 800  
 Smith, B. A., & Terrile, R. J. 1984, *Science*, 226, 1421  
 Soubiran, C., Le Campion, J.-F., Cayrel de Strobel, G., & Caillo, A. 2010, *A&A*, 515, A111  
 Sousa, S. G., Santos, N. C., Israelian, G., Lovis, C., Mayor, M., Silva, P. B., & Udry, S. 2011a, *A&A*, 526, A99  
 Sousa, S. G., Santos, N. C., Israelian, G., Mayor, M., & Udry, S. 2011b, *A&A*, 533, A141  
 Sousa, S. G., et al. 2008, *A&A*, 487, 373  
 Su, K. Y. L., et al. 2005, *ApJ*, 628, 487  
 Su, K. Y. L., et al. 2013, *ApJ*, 763, 118  
 Suchkov, A. A., Makarov, V. V., & Voges, W. 2003, *ApJ*, 595, 1206  
 Takeda, Y., Kang, D.-I., Han, I., Lee, B.-C., & Kim, K.-M. 2009, *PASJ*, 61, 1165

Takeda, Y., Ohkubo, M., Sato, B., Kambe, E., & Sadakane, K. 2005, *PASJ*, 57, 27  
 Taylor, B. J. 2005, *ApJS*, 161, 444  
 Thébault, P., Augereau, J. C., & Beust, H. 2003, *A&A*, 408, 775  
 Theil, H. 1950, *Nederl. Akad. Wetensch., Proc.*, 53, 386  
 Thureau, N. D., et al. 2014, *MNRAS*, 445, 2558  
 Trilling, D. E., et al. 2008, *ApJ*, 674, 1086  
 Valenti, J. A., & Fischer, D. A. 2005, *ApJS*, 159, 141  
 Wang, J., & Fischer, D. A. 2015, *AJ*, 149, 14  
 Wang, J., Fischer, D. A., Horch, E. P., & Huang, X. 2015, *ApJ*, 799, 229  
 Wright, J. T., & Gaudi, B. S. 2013, *Exoplanet Detection Methods*, ed. T. D. Oswalt, L. M. French, & P. Kalas, 489  
 Wu, C.-J., Wu, H., Lam, M.-I., Yang, M., Wen, X.-Q., Li, S., Zhang, T.-J., & Gao, L. 2013, *ApJS*, 208, 29  
 Wu, Y., Singh, H. P., Prugniel, P., Gupta, R., & Koleva, M. 2011, *A&A*, 525, A71  
 Wyatt, M. C. 2008, *ARA&A*, 46, 339  
 Wyatt, M. C., Smith, R., Su, K. Y. L., Rieke, G. H., Greaves, J. S., Beichman, C. A., & Bryden, G. 2007, *ApJ*, 663, 365